Mathematical Sciences Faculty Publications

2006

Clefting in a Pumpkin Balloon

K. A. Brakke
Susquehanna University

Frank E. Baginski
The George Washington University Law School

Willi W. Schur

Recommended Citation

F. Baginski, K. Brakke, and W. Schur, Cleft formation in pumpkin balloons, Advances in Space Research 37 no. 11 (2006) 2070-2081.

CLEFTING IN A PUMPKIN BALLOON

Frank E. Baginski[a]*, Kenneth A. Brakke[b], and Willi W. Schur[c]

[a]Department of Mathematics, The George Washington University
Washington, DC 20052, USA

[b]Mathematics Department, Susquehanna University,
Selinsgrove, PA 17870, USA

[c]P.O. Box 698,
Accomac, VA 23301, USA

NASA's development of a large payload, high altitude, long duration balloon, the Ultra Long Duration Balloon, centers on a pumpkin shape super-pressure design. Under certain circumstances, it has been observed that a pumpkin balloon may be unable to pressurize into the desired cyclically symmetric equilibrium configuration, settling into a distorted, undesired state instead. Long term success of the pumpkin balloon for NASA requires a thorough understanding of the phenomenon of multiple stable equilibria and means for quantitative assessment of measures that prevent the occurrence of undesired equilibrium. In this paper, we will use the concept of stability to classify equilibrium shapes of fully pressurized/fully deployed strained balloons. Our mathematical model for a strained equilibrium balloon, when applied to a shape that mimics the Phase IV-A balloon of Flight 517, predicts instability at float. Launched in Spring 2003, this pumpkin balloon failed to deploy properly. Small scale testing suggests that increasing the number of gores n_g and utilizing a minimal bulge radius increases the likelihood of deployment problems. Hoop stress considerations in the pumpkin design lead to choosing the lowest possible bulge radius r_B, while robust deployment is favored by a large bulge radius. In an effort to quantify this dependency, we will explore the stability of a family of balloon shapes parametrized by (n_g, r_B) which includes a design that is very similar, but not identical, to the balloon of Flight 517. In addition, we carry out a number of simulations that demonstrate other aspects related to multiple equilibria of pumpkin balloons.

1. Introduction

NASA's Phase II and Phase III Ultra Long Duration Balloons (ULDB) were *constant bulge radius* pumpkin designs (see [1]) that fully deployed once they reached their respective float altitudes. Other factors shortened the length of these missions, but here we are concerned with deployment related issues only. See [2] for more on ULDB flights. The Phase II pumpkin had a volume of 51,450 cubic meters and 145 gores. The Phase III pumpkin had a volume of 68,526 cubic meters and 150 gores. During test flights for the NASA Phase IV-A design, a much larger balloon with 290 gores and a volume of about 0.6 million cubic meters, the balloon did not fully deploy in Flight 517. A cleft that was observed in the launch configuration, was maintained throughout the ascent phase, and remained once the balloon reached maximum altitude. See Figure 1(a) for a snap-shot of the Flight 517 cleft. Testing of small scale balloons under constant pressure at sea level in a controlled environment suggest that increasing the number of gores n_g,

Figure 1. (a) Flight 517 Cleft (Photograph courtesy of the NASA Balloon Program Office); (b) Pumpkin gore with lay-flat configuration.

(a)   (b)
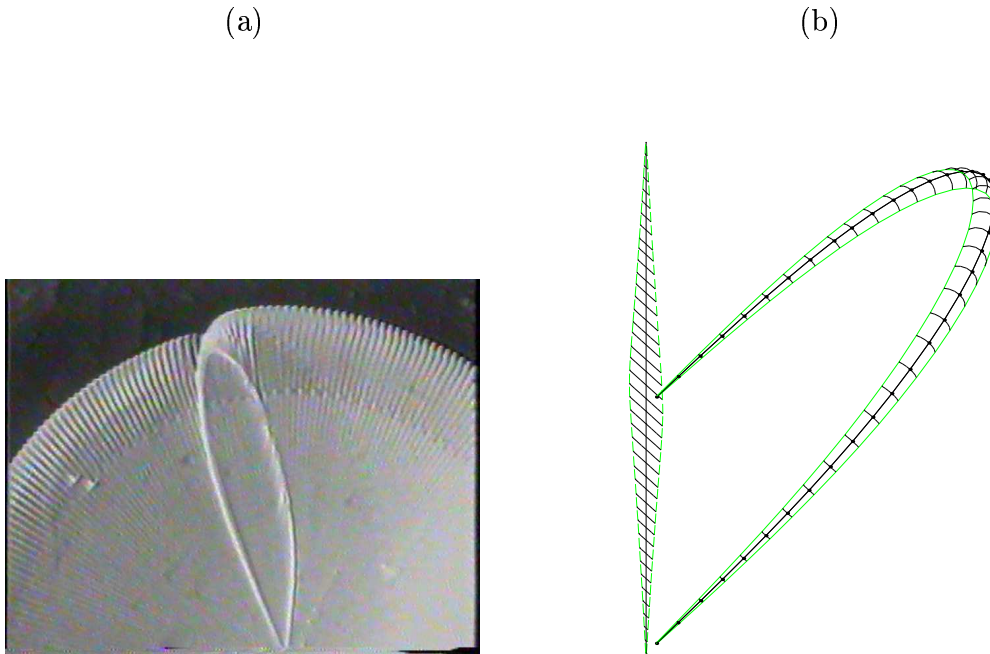
increases the likelihood of deployment problems. Furthermore, adding sufficient extra material to the gore width can also lead to an undesired equilibrium configuration, even when the balloon is fully pressurized. Ground tests suggest that the location of the extra gore width is also important. Extra gore width added near the mid-latitudes is more likely to lead to a deployment problem than extra gore-width added near the equator. See [3] for more on tests involving small pumpkin balloons.

In the 1980's during the race for the first circumnavigation of the globe, Julian Nott was one of the first researchers to tackle the problem of undesired equilibrium shapes in a pumpkin type balloon. Nott's vehicle, called the *Endeavour*, was a 64 gore *constant bulge shape* pumpkin balloon. By constant bulge shape, we mean that the radial rays that bound the circular bulge sweep the same angle anywhere along the gore. When fully pressurized during ground tests, the *Endeavour* did not attain the desired configuration and only after 4 gores were removed did it attain a cyclically symmetric equilibrium configuration. Using a stability analysis based on the hydrostatic pressure potential energy and ignoring strain energy, researchers in [4] and [5] attempted to explain the failure of the *Endeavour* to achieve the equilibrium state that was intended.

In the present work, we will consider the stability of equilibrium configurations of pumpkin balloons, where the balloon system is modeled as an elastic membrane with load tendons. Wrinkling of the membrane is modeled by energy relaxation. The total energy of the balloon includes the hydrostatic pressure potential, film and tendon gravitational potential energy, film strain energy and tendon strain energy. We calculate equilibrium configurations via an energy minimizing approach (see Section 2) and then carry out a stability analysis of equilibria that were found. If $H(\mathcal{S})$ is the Hessian of the potential energy of the balloon evaluated at equilibrium configuration $\mathcal{S}$, then we say $\mathcal{S}$ is stable if all the eigenvalues of $H(\mathcal{S})$ are positive. See Section 3 for the definition of stability. Our stability results are compared with the Calledine stability results and available experimental data in Section 4.4.

In Section 4.3, we present a detailed analysis of a two-parameter family of pumpkin balloons

that includes a balloon design that is similar to that of the balloon used in Flight 517. We find that the fully inflated/fully deployed configuration of our model that mimics the balloon of Flight 517 is unstable. In fact, this configuration is right on the border separating the stable and unstable equilibria. In addition, we analyzed a shape that was based on the lay-flat pattern and tendon local lack-of-fit that was used in the construction of Flight 517's balloon. We found this equilibrium shape, as well, to be unstable under float conditions. See Section 4.1.

One of the difficulties analyzing pumpkin balloons with significant excess material is handling regions of self-contact. In Section 4.5, we consider a pumpkin balloon with significant excess material, so much so, that it is impossible for the balloon to assume a cyclically symmetric equilibrium shape.

It is probably safe to say that the number of gores and the bulge radius in a pumpkin design are important design parameters. However, there is very little experimental data available that allows one to characterize how a change in one of these parameters will affect the stability of a corresponding equilibrium configuration. Keeping in mind the assumptions made, Callendine's stability approach is a reasonable first estimate. However, our model is more comprehensive and provides a more detailed picture of the stability, including parameter dependencies.

2. Finite element model

In this section, we formulate the problem of determining the equilibrium shape of a strained balloon. We have applied this model to pumpkin balloons and we refer the reader to [7] for a more detailed exposition.

In the following, we will assume that a balloon is situated in such a way that the theoretical center of the bottom of the pneumatic envelope is the origin of a Cartesian coordinate system. A balloon has n_g gores and we assume that $y = 0$ is a plane of reflectional symmetry. The nadir fitting is fixed, and the apex fitting is free to slide up and down the z-axis. The nadir fitting and the apex fitting are assumed to be rigid. The total potential energy $\mathcal{E}$ of a strained inflated balloon configuration $\mathcal{S}$ is the sum of six terms,

$$\mathcal{E}(\mathcal{S}) = \mathcal{E}_P + \mathcal{E}_f + \mathcal{E}_t + \mathcal{E}_{top} + S_t^* + S_f^* \tag{1}$$

where

$$\mathcal{E}_P(\mathcal{S}) = -\int_{\mathcal{S}} (\tfrac{1}{2}bz^2 + P_0 z)\mathbf{k} \cdot d\vec{S}, \tag{2}$$

$$\mathcal{E}_f(\mathcal{S}) = \int_{\mathcal{S}} w_f z\, dA, \tag{3}$$

$$\mathcal{E}_t(\mathcal{S}) = \int_{\Gamma \in \mathcal{S}} w_t \boldsymbol{\tau}(s) \cdot \mathbf{k} \ ds, \tag{4}$$

$$\mathcal{E}_{top}(\mathcal{S}) = w_{top} z_{top}, \tag{5}$$

$$S_f^*(\mathcal{S}) = \int_{\mathcal{S}} W_f^* \, dA, \tag{6}$$

$$S_t^*(\mathcal{S}) = \int_{\Gamma \in \mathcal{S}} W_t^* \, ds, \tag{7}$$

$\mathcal{E}_P$ is the hydrostatic pressure potential due to the lifting gas, $\mathcal{E}_f$ is the gravitational potential energy of the film, $\mathcal{E}_t$ is the gravitational potential energy of the load tendons, $\mathcal{E}_{top}$ is the gravitational potential energy of the apex fitting, S_t^* is the relaxed strain energy of the tendons, and S_f^* is the relaxed strain energy of the balloon film, P_0 is the differential pressure at the base of the balloon where $z = 0$, b is the specific buoyancy of the lifting gas, $d\vec{S} = \mathbf{n}\, dS$, $\mathbf{n}$ is the outward unit normal, dS is surface area measure on the strained balloon surface, w_f is the film weight per unit area, w_t is the tendon weight per unit length, $\boldsymbol{\tau} \in \mathbb{R}^3$ is a parametrization of a deformed tendon $\Gamma \in \mathcal{S}$, w_{top} is the weight of the apex fitting, z_{top} is the height of w_{top}, W_f^* is the relaxed film strain energy density, W_t^* is the relaxed tendon strain energy density. Relaxation

of the film strain energy density is a way of modeling wrinkling in the balloon film and has been used in the analysis of pumpkin shaped balloons in [7].

To determine a strained equilibrium balloon shape, we solve the following,

$$\text{Problem } \star: \quad \min_{\mathcal{S} \in \mathcal{C}} \mathcal{E}(\mathcal{S}).$$

$\mathcal{C}$ denotes the class of feasible balloon shapes. Boundary conditions are built into $\mathcal{C}$. In the present work, we will assume the differential pressure is in the form $P(z) = -bz - P_0$ and that P_0 is known. We follow the convention that $-P(z) > 0$ means that the internal pressure is greater than the external pressure. Here, the continuum problem is cast as an optimization problem. This approach is particularly well-suited for the analysis of compliant structures. Problem $\star$ was implemented into *Surface Evolver*, a C-program developed by the second author (see [8]). *Surface Evolver* is a software package for interactive study of curves and surfaces shaped by energy minimization. We used *Surface Evolver* to calculate solutions of Problem $\star$ and to determine the stability of the solutions found.

3. Stability

The degrees of freedom (DOF) in a faceted balloon shape $\mathcal{S}$ are the coordinates of the facet nodes that are free to move. Let $\boldsymbol{x} = (x_1, x_2, \ldots, x_N)$ be a list of the DOF. Let $\mathcal{E}(\boldsymbol{x})$ be the total energy of a balloon configuration $\mathcal{S} = \mathcal{S}(\boldsymbol{x})$. The Hessian of $\mathcal{E}$ evaluated at $\boldsymbol{x}$ is the $N \times N$ matrix of second order partial derivatives of $\mathcal{E}$,

$$H_{\mathcal{E}}(\mathcal{S}) \stackrel{\text{def}}{=} H_{\mathcal{E}}(\boldsymbol{x}) = \left[\frac{\partial^2 \mathcal{E}}{\partial x_i \partial x_j}(\boldsymbol{x}) \right], \quad i = 1, 2, \ldots, N, \quad j = 1, 2, \ldots, N. \tag{8}$$

When a volume constraint is imposed, Eq. (8) must be modified. Depending on the mesh size and number of gores, N is between 85,000 and 350,000 in our studies. However, H is sparse. The lowest eigenvalue of H was calculated by inverse iteration. The matrix $H - tI$ was sparse Cholesky factored, with the shift value t chosen to guarantee positive definiteness. The factored matrix was then used to iteratively solve $(H - tI)\boldsymbol{x}_(n + 1) = \boldsymbol{x}_n$, starting with a random vector $\boldsymbol{x}_0$, until the iteration converged, almost certainly producing the eigenvector of the lowest eigenvalue. See [10, Section 11.7, p. 493].

Next, we define the stability of an equilibrium shape $\mathcal{S}$.

Definition 3.1 *Let $\mathcal{S} = \mathcal{S}(\boldsymbol{x})$ be an equilibrium configuration, i.e., a solution of Problem $\star$. We say $\mathcal{S}$ is* stable *if all the eigenvalues of $H_{\mathcal{E}}(\mathcal{S})$ are positive. We say $\mathcal{S}$ is* unstable *if at least one eigenvalue of $H_{\mathcal{E}}(\mathcal{S})$ is negative. We say that the stability of $\mathcal{S}$ is* indeterminate *if the lowest eigenvalue of $H_{\mathcal{E}}(\mathcal{S})$ is zero.*

4. Parametric Studies

We begin by giving an overview of the shape finding process and the setup of Problem $\star$. We will focus most of our attention on designs related to Flight 517. Parameters relevant to the Flight 517 design are given in Table 1.

There are twelve parameters that go into the shape finding process for a pumpkin balloon: number of gores ($p_1 = n_g$), bulge radius ($p_2 = r_B$), constant pressure term ($p_3 = P_0$), buoyancy of lifting gas ($p_4 = b$), length of Cap 1 ($p_5 = c_1$), length of Cap 2 ($p_6 = c_2$), film weight density ($p_7 = w_f$), Cap 1 weight density ($p_8 = w_{c_1}$), Cap 2 weight density ($p_9 = w_{c_2}$), tendon weight density ($p_{10} = w_t$), suspended payload ($p_{11} = L$, includes weight of nadir fitting), and apex fitting weight ($p_{12} = w_{top}$). See [1] for more on the pumpkin model. Typically, material

Table 1

(a) Shape finding parameters		
Description	Variable	Nominal Value
Number of gores	$p_1 = n_g$	290
Bulge radius	$p_2 = r_B$	0.78 m
Constant pressure term	$p_3 = P_0$	130 Pa
Buoyancy	$p_4 = b$	0.087 N/m^3
Cap 1 length	$p_5 = c_1$	50 m
Cap 2 length	$p_6 = c_2$	55 m
Tendon weight density	$p_7 = w_t$	0.094 N/m
Film weight density	$p_8 = w_f$	0.344 N/m^2
Cap 1 weight density	$p_9 = w_{c_1}$	0.184 N/m^2
Cap 2 weight density	$p_{10} = w_{c_2}$	0.184 N/m^2
Payload	$p_{11} = L$	27.80 kN
Top fitting weight	$p_{12} = w_{top}$	0.79

(b) Material properties for strained equilibrium		
Description	Variable	Value
Film Youngs modulus	$q_1 = E_f$	404.2 MPa
Film Poisson ratio	$q_2 = \nu_f$	0.830
Cap 1 Youngs modulus	$q_3 = E_{c_1}$	216 MPa
Cap 1 Poisson ratio	$q_4 = \nu_{c_1}$	0.830
Cap 2 Youngs modulus	$q_5 = E_{c_2}$	216 MPa
Cap 2 Poisson ratio	$q_6 = \nu_{c_2}$	0.830
Tendon stiffness	$q_7 = E_t$	0.650 MN
Tendon slackness	$q_8 = \epsilon_t$	−0.008 m/m

properties such film modulus and Poisson ratio do not enter directly into the shape finding process. We define the shape finding vector, to be

$$
\begin{aligned}
\boldsymbol{p} &= (p_1, p_2, \ldots, p_{12}) \\
&= (n_g, r_B, P_0, b, c_1, c_2, w_f, w_{c_1}, w_{c_2}, w_t, L, w_{top}).
\end{aligned}
\tag{9}
$$

The shape finding parameters that were used for the Flight 517 design are presented in Table 1(a). Once a set of values are assigned to $\boldsymbol{p}$, the pumpkin design shape $\mathcal{S}_d(\boldsymbol{p}) \subset \mathbb{R}^3$ and the corresponding lay-flat pattern $\Omega(\boldsymbol{p}) \subset \mathbb{R}^2$ are determined. For Flight 517, we find that the volume is 0.59 million cubic meters, the tendon length is 155.30 m and the gore seam length is 155.93 m.

The three-dimensional shape $\mathcal{S}_d(\boldsymbol{p})$ is discretized (call it $\mathcal{S}_d(\boldsymbol{x}; \boldsymbol{p})$), and $\mathcal{S}_d(\boldsymbol{x}; \boldsymbol{p})$ is used as the initial guess for solving Problem $\star$ and determining the corresponding strained equilibrium shape, denoted by $\mathcal{S}(\boldsymbol{x}; \boldsymbol{p})$ or $\mathcal{S}(\boldsymbol{p})$. The tendon length is the edge length of $\mathcal{S}_d(\boldsymbol{p})$. By construction, the edge of the lay-flat pattern $\Omega(\boldsymbol{p})$ is longer than the tendon length. To accommodate this lack-of-fit, the film along the seam is gathered before the tendon is attached. Note, local lack-of-fit varies along the length of the seam (i.e., more material must be gathered near the equator than near the gore end).

If the unstrained tendon has no slackness, each segment length in the tendon should match the corresponding length in $\mathcal{S}_d$. However, to model the tendon/film mismatch properly, we should allow for tendon slackness or additional tendon shortening and so we introduce the tendon uniform slackness parameter ϵ_t. In particular, if $\epsilon_t = 0.005$, then a tendon segment must strain 0.5% before it comes under tension. If $\epsilon_t = -0.005$, then each tendon segment length is shortened by an additional 0.5% beyond the local lack-of-fit due to the $\mathcal{S}_d(\boldsymbol{p})$ and $\Omega(\boldsymbol{p})$ mismatch. In theory, $\epsilon_t = 0$, but to illustrate sensitivity to this parameter, we set $\epsilon = -0.008$ for the nominal case.

We are most interested in investigating the stability of equilibria of pumpkin designs as a function of (n_g, r_B), and for this reason, we define the following family of balloon designs

$$\Pi_d = \{\{\mathcal{S}_d(\boldsymbol{p}), \Omega(\boldsymbol{p})\}, p_1 \in \{48, 49, \ldots, 350\}, \bar{r}_B(p_1) < p_2 < \infty, \ p_3, p_4, \ldots, p_{12} \text{ see Table 1(a)}\} (10)$$

where $\bar{r}_B(n_g)$ is the minimal bulge radius for a design with n_g gores. For convenience, we will refer to a particular design in Π_d, by indicating the number of gores and the bulge radius. For example, $\{\mathcal{S}_d(290, 0.78), \Omega(290, 0.78)\}$ refers to the Flight 517 design. If a parameter is not explicitly written out, it will be our convention that it is assigned the value in Table 1. Note, most of these designs are not practical. Analyses of these cases merely allow exploration that aid our understanding of the causes of the instabilities that are of concern.

Once a design has been defined, then we can carry out a stress analysis of that design for some applied load. Coming into play at this stage are other properties such as the film Youngs modulus ($q_1 = E_f$), film Poisson ratio ($q_2 = \nu_f$), Cap 1 Youngs modulus ($q_3 = E_{c_1}$), Cap 1 Poisson ratio ($q_4 = \nu_{c_1}$), Cap 2 Youngs modulus ($q_5 = E_{c_2}$), Cap 2 Poisson ratio ($q_6 = \nu_{c_2}$), tendon stiffness ($q_7 = E_t$), and the tendon slackness parameter ($q_8 = \epsilon_t$). We define

$$\begin{aligned} \boldsymbol{q} &= (q_1, q_2, \ldots, q_8) \\ &= (E_f, \nu_f, E_{c_1}, \nu_{c_1}, E_{c_2}, \nu_{c_2}, E_t, \epsilon_t). \end{aligned} \qquad (11)$$

Nominal values for $\boldsymbol{q}$ are presented in Table 1(b). Once $\boldsymbol{p}$ and $\boldsymbol{q}$ are specified, we can proceed to the problem of solving Problem $\star$. Note, the shape determination process and the solution of Problem $\star$ are separate processes, and so it possible to use $\boldsymbol{p}$ in the shape finding process, and vector $\boldsymbol{p}'$ in the solution of Problem $\star$. While $\boldsymbol{p}$ is usually chosen with a particular $\boldsymbol{q}$ in mind, one might also use another vector $\boldsymbol{q}'$ in the solution of Problem $\star$. The shape finding process and $\boldsymbol{p}$ defines the lay-flat gore pattern $\Omega(\boldsymbol{p})$ and provides a three dimensional shape $\mathcal{S}_d(\boldsymbol{p})$ that is used for determining the strained equilibrium shape which will be denoted by $\mathcal{S}(\boldsymbol{p}', \boldsymbol{q}', \Omega(\boldsymbol{p}))$. In our stability studies involving Π_d, we will consider nominal parameter values for $\boldsymbol{q}$. After solving Problem $\star$ with a design $\{\mathcal{S}_d, \Omega\} \in \Pi_d$, we will then classify the resulting strained equilibrium configuration $\mathcal{S}$ according to Definition 3.1.

4.1. Analysis of Flight 517 Design

Although the gore pattern generated by the model in [1] was very close to the pattern used by the manufacturer to build the Phase IV-A balloon, we thought it prudent to analyze a shape that was as close as possible to the fabricated Phase IV-A balloon. For this reason, we obtained the gore pattern and tendon lack-of-fit that was used to build the Flight 517 balloon and input these data into our model along with the parameters as presented in Table 1. We found that the equilibrium shape using this design for float conditions and nominal parameters was unstable by Definition 3.1. We reduced the number of gores to 282, retained the same gore pattern, and found that the corresponding equilibrium shape was stable. This suggests that stability is sensitive to extra gore width material.

4.2. Molded Super-gore

Since our model predicted that the Flight 517 balloon was unstable, we considered a pumpkin design that was based on the "molded super-gore" construction discussed in [9]. In the molded super-gore approach, one achieves the effect of a molded gore by seaming together a number of different long flat warped sheets of film. After seaming together the warped panels, the resulting super-gore edge has the proper length so that local film/tendon lack-of-fit is not necessary. In this particular study, we assumed the balloon had 288 gores. We found that the nominal pumpkin balloon led to an unstable equilibrium configuration at float conditions. On the other hand, a pumpkin balloon, using the molded super-gore construction, was found to be stable at float. See Table 2. While the molded super-gore construction is not feasible for large pumpkin balloons, there are applications, such as small planetary balloon missions, where the additional time and fabrication costs are worthwhile (see [9]).

Table 2

Stability of a nominal pumpkin balloon with one lay-flat panel per gore versus a pumpkin balloon based on a molded super-gore construction.

Pumpkin gore design	Nominal	Molded
Lowest eigenvalue of $H_{\mathcal{E}}$	-1.478	0.857

4.3. A two parameter family of designs.

To investigate the sensitivity of a pumpkin balloon equilibrium shape to a change in the number of gores or the bulge radius, we generated a family of shapes Π_d, using the default values in Table 1 and varied (n_g, r_B). We then computed an equilibrium configuration for each design, modeling one-half of the balloon. Each equilibrium configuration was classified as stable or unstable according to Definition 3.1. The results are plotted in Figure 2. A stable equilibrium $\mathcal{S}(n_g, r_B)$ is covered by a square and an unstable equilibrium is covered by a dot. Note the location of $\mathcal{S}(290, 0.78)$ (the shape that mimics the balloon of Flight 517) is on the border between stable and unstable equilibria. See Figure 2.
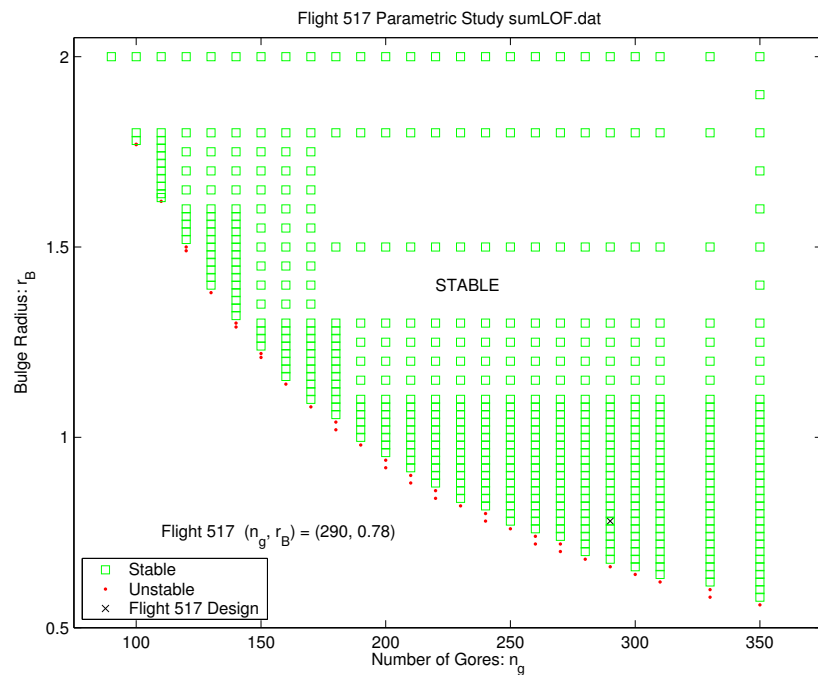
If there is no additional fore-shortening in the unstrained tendon and there is no slackness in the tendons, $\epsilon_t = 0$. We analyzed the designs in Π_d using nominal parameter values in Table 1, except we set $\epsilon_t = 0$. The results are plotted in Figure 3, where we see that the region of unstable equilibria has been reduced, but not eliminated. Note, in Figure 3, we have plotted $100 \le n_g \le 350$ and $0.5 < r_B < 2.1$.

4.4. Comparisons with experimental data

In an earlier work, Calledine investigated the stability of pumpkin shape super-pressure balloons of the constant bulge shape design and presented his findings in a formula for a stability limit. Plotting Callendine's formula, M. Smith of Raven Industries compared several pumpkin balloons of different design schemes to Calledine's stability limit. This comparison was reproduced and added to in [3, Figure 5]. We have included this presentation in Figure 4, and have added our findings for nominally constant bulge radius designs. We designate stable designs by square symbols and unstable designs by stars. Our stability limit is the border separating the symbols for stable and unstable designs.

We note that Calledine investigated the behavior of constant bulge shape balloons via a two dimensional proxi-model. He calibrated the formulation obtained from his model on a few data points obtained from a constant bulge shape balloon. His stability limit is a curve in a two-parameter plot. The parameters are the ratio (S/C) and the number of gores. C is the chord distance between adjacent tendons. The arc length between adjacent tendons as measured along the bulging gore is denoted by S. Calledine predicts that constant bulge shape designs that fall below his limit line are stable and those that fall above the limit line are unstable. In the case of a constant bulge shape design the ratio S/C is a constant. We include constant bulge radius designs by plotting against the ratio max(S/C) which occurs at the equator.

Calledine's derivation of the formulation for the stability limit was based on an inextensional model for which there is no strain energy hence there is no second variation of strain energy. He observed that for such a case, the principal of the Minimum Total Potential Energy reduces for a pneumatic envelope to a maximum volume rule. This rule is exact for the fictitious case of inextendable materials and within limits approximate in the case of elastic materials with very little compliance. It worked well for Calledine in his semi-empirical investigation where the structural materials of the pneumatic envelope were fixed. Given the analytical capability of the era, Callendine's simplification was enabling. We also note that a constant bulge shape design by Raven Industries falling near Calledine's stability limit exhibited at (supposedly) the

Figure 2. Regions of stability for Π_d variations on Flight 517 baseline.

Phase IV–A Parametric Study sumNOM.dat
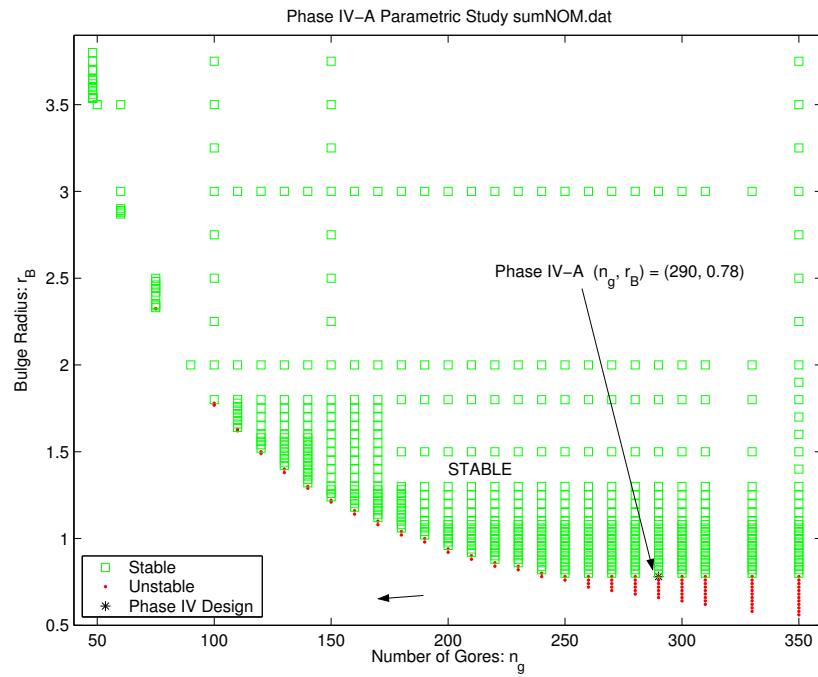
Figure 3. Regions of stability for Π_d variations on Flight 517 baseline with $\epsilon_t = 0$.

Flight 517 Parametric Study sumLOF.dat

design pressure robust stable behavior but under further pressurization became unstable and migrated into a distorted equilibrium shape. The structural materials of the Raven balloon were different from those for the balloon used by Calledine for calibration. This is remarkable. There is, however, reason to assert that in the case of elastomeric materials the approximate rule would fail even in a semi-empirical investigation.

Included in Figure 3 are the Phase II, Phase III, and Phase IV-A balloons of NASA's ULDB program and a number of 48 gore test vehicles. The Phase II and Phase III balloons deployed properly. Of two Phase IV-A balloons, the first flown in Summer 2002 in Palestine, Texas deployed. The second, Flight 517NT flown in Spring 2003 in Australia failed to fully deploy. After launch it displayed a large primary cleft that did not fully disengage when reaching float altitude. The designs of both Phase IV-A balloons were identical. We note that there are, of course, fabrication induced variations from balloon to balloon. Both, the Phase II and the Phase III balloons were nominally constant bulge radius designs. They are inside or near the stable territory of Calledine's stability plot for constant bulge shape designs. The Phase IV-A balloons, also nominally constant bulge radius designs, are inside or near unstable territory for Callendine's stability curve. Our investigation places the Phase IV-A balloon right at the border that separates stable designs from unstable designs.

There are a number of 48 gore test vehicles plotted on Figure 3. Some of them deployed properly, some did not. The designs of these test vehicles differed from each other both in bulge radius and bulge radius distribution over the gore length. In each case, however, max(S/C) occurs at the equator. The purpose of this minimal test program was to learn what features of gore design are most and least detrimental to proper deployment.

4.5. Extreme geometries

Suppose we are given a gore pattern $\Omega(\boldsymbol{p})$ based on shape finding vector $\boldsymbol{p}$ with $p_1 = n_g$. If we increase the number of gores in the "fabricated balloon" sufficiently high (i.e., choose $p_1' >> p_1$), and then attempt to inflate that balloon, it is unlikely that one will observe a cyclically symmetric shape. This is akin to what Julian Nott observed in the *Endeavour*. Similar shapes can also be observed in some of the experiments in [3]. Computationally, this is a difficult problem to model due to the balloon coming into self-contact. Partially inflated natural-shape balloons with significant regions of self-contact were studied in [6]. However, the ascent configurations of zero-pressure balloons have "fin-like" structures where excess film can fold up in a very natural way. To demonstrate the complexity of modeling this scenario for pumpkin balloons with significant excess material, we generated a gore pattern Ω for a 6.6 meter diameter pumpkin balloon with bulge radius $r_B = 0.112$ m and $n_g = 96$. However, instead of using 96 copies of Ω to assemble the balloon, we used 128 copies. The constant pressure term was $P_0 = 200$ Pa, but under this load (or any realistic load), the resulting equilibrium shape is quite complicated. We computed one representative shape to demonstrate our capabilities. We assumed that the 128 gore balloon had D_4 dihedral symmetry, i.e., four symmetric large scale lobes. Each large scale lobe consisted of 32 gores that were symmetric about a bisecting plane that contained the z-axis. Thus, we needed to model only 16 gores. The equilibrium shape computed with 16 gores was unstable. A 16-gore half-lobe is shown in Figure 5. The complete shape is shown in Figure 6. Note, there is significant excess material in this configuration. Increasing the pressure will not yield a cyclically symmetric shape. Unlike the ascent shapes of zero-pressure balloons where excess material appears to hang in vertical planes containing the fin-like structures, Figure 6 appears to have a twisting mode.

5. Conclusions

While the results presented in this paper are not sufficient to predict whether a particular balloon design will or will not deploy, instability of the fully inflated/fully deployed strained equilibrium configuration at float conditions appears to be an indicator for an unfavorable deployment. The balloon designer is inviting trouble if a selected design leads to an unstable equilibrium configuration at float. For if the desired float shape is a cyclically symmetric un-

Figure 4. Comparison of BBS-stability and Calledine stability. Calledine stability curve is reproduced from [3, Figure 5]. Additional experimental and flight data are annotated in the figure. D-deployed; F-failed deployment.
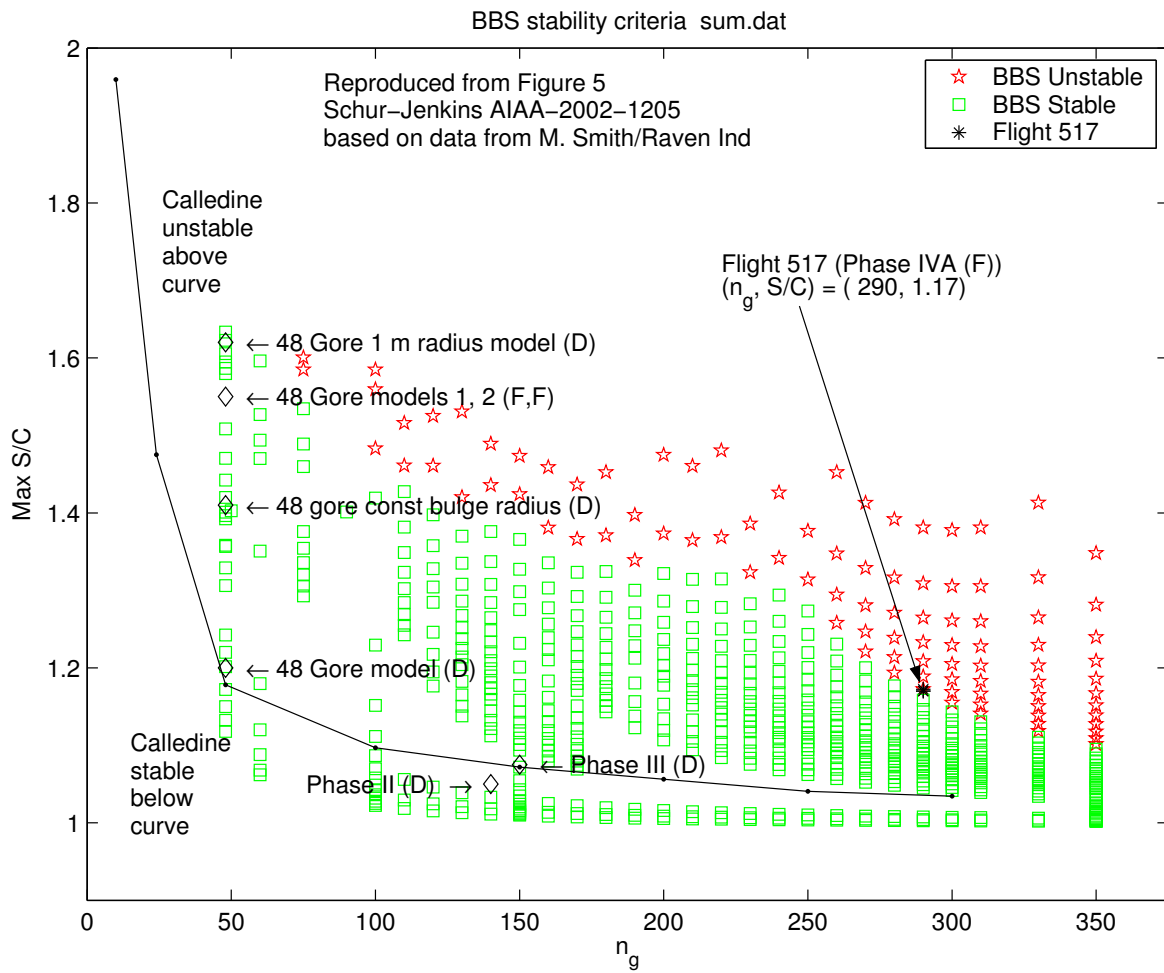
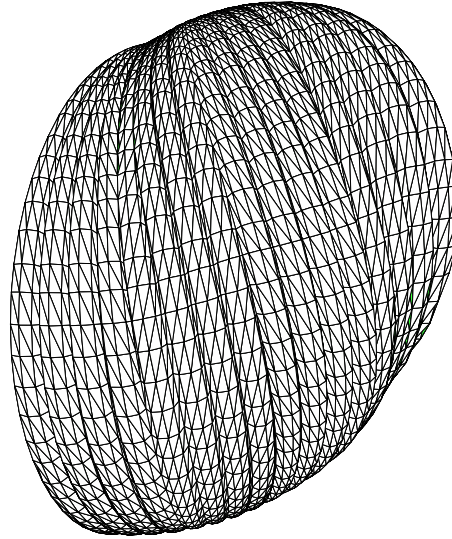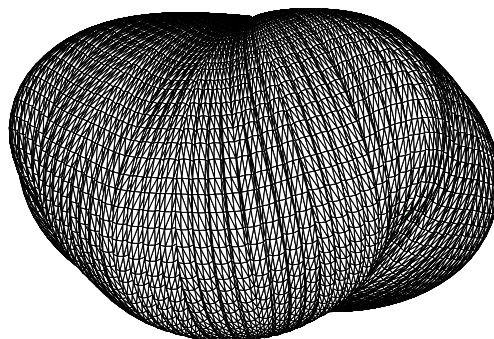Figure 5. One-eighth of an unstable equilibrium configuration of a 128 gore balloon.

Figure 6. An unstable equilibrium configuration of a 128 gore balloon.

stable equilibrium configuration, and the real balloon corresponds, in all aspects including the pressurization state to the analytical model, then the balloon should not even be able to attain that cyclically symmetric float shape through a normal ascent. The successful deployment of the Phase II and Phase III balloons, and the failed deployments of Phase IV and Phase IV-A type balloons support our assertion. Ultimately, it would be desirable to develop guidelines and dependable tools that would enable the balloon designer to a determine the proper balloon that will safely and reliably meet the flight requirements for a long duration balloon mission, including proper deployment. Although not all the necessary preliminaries are provided in this paper, our results support the case that the development of such design aids is within reach.

REFERENCES

1. F. Baginski, "On the design and analysis of inflated membranes: natural and pumpkin shaped balloons," to appear in the SIAM Journal on Applied Mathematics.

2. F. Baginski and W. Schur, "Undesired equilibria of self-deploying pneumatic envelopes," AIAA-2004-1734, 45th AIAA/ASME/ASCE/AHS/ASC Structures, Structural Dynamics & Materials Conference, Palm Springs, CA, April 2004.

3. W. W. Schur , and C. H. Jenkins, "Deployment destiny, stable equilibria, and the implications for gossamer design," AIAA-2002-1205, 43nd AIAA/ASME/ ASCE/AHS/ASC Structures, Structural Dynamics and Materials Conference and Exhibit, Denver, CO, April 2002.

4. C. R. Calledine, "Stability of the Endeavour Balloon" in Buckling of Structures, I. Elishakoff et al. (eds.), Elsevier Science Publishers, (1988) 133-149.

5. A. Lennon and S. Pellegrino, "Stability of Lobed Inflatable Structures," AIAA-2000-1728, 41st AIAA/ASME/ASCE/AHS/ASC Structural Dynamics, and Materials Conference and Exhibit, Atlanta, GA, April 2000.

6. F. Baginski, "Non-uniqueness of strained ascent shapes of high altitude balloons," Adv. Space Res., **33** No. 10 (2004), 1705-1710.

7. F. Baginski and W. Schur, "Structural Analysis of Pneumatic Envelopes: A Variational Formulation and Optimization-Based Solution Process," *AIAA J.*, **41** No. 2 (2003) 304-311.

8. K. Brakke, *The surface evolver*, Experimental Mathematics **1**:2 (1992) 141-165.

9. F. Baginski and W. Schur, "Design Issues for Large Scientific Balloons," AIAA-2003-6788, 3rd Annual Aviation Technology, Integration, and Operations (ATIO) Technical Forum, Denver, CO, October 2003.

10. W. Press et al, Numerical Recipes in C, 2nd ed., Cambridge University Press, 1992.